Received: 2 June 2018 | Revised and accepted: 13 June 2018

DOI: 10.1111/jns.12278

WILEY

RESEARCH REPORT

A unified model of the excitability of mouse sensory and motor axons

Preet G. S. Makker[1] | José M. Matamala[2] | Susanna B. Park[2] | Justin G. Lees[1] | Matthew C. Kiernan[2,3] | David Burke[3] | Gila Moalem-Taylor[1] | James Howells[2]

[1]School of Medical Sciences, University of New South Wales, Sydney, Australia

[2]Brain and Mind Centre, The University of Sydney, Sydney, Australia

[3]Royal Prince Alfred Hospital, The University of Sydney, Sydney, Australia

Correspondence
James Howells, Brain and Mind Centre, The University of Sydney, 94 Mallett Street Camperdown, Sydney, NSW 2050, Australia.
Email: james.howells@sydney.edu.au

Funding information
Motor Neurone Disease Research Institute of Australia, Grant/Award Number: BGF14 for 2015-2017; Cancer Institute NSW, Grant/Award Number: 14/TPG/1-05; National Health and Medical Research Council of Australia (NHMRC), Grant/Award Number: 1037746

Non-invasive nerve excitability techniques have provided valuable insight into the understanding of neurological disorders. The widespread use of mice in translational research on peripheral nerve disorders and by pharmaceutical companies during drug development requires valid and reliable models that can be compared to humans. This study established a novel experimental protocol that enables comparative assessment of the excitability properties of motor and sensory axons at the same site in mouse caudal nerve, compared the mouse data to data for motor and sensory axons in human median nerve at the wrist, and constructed a mathematical model of the excitability of mouse axons. In a separate study, ischaemia was employed as an experimental manoeuvre to test the translational utility of this preparation. The patterns of mouse sensory and motor excitability were qualitatively similar to human studies under normal and ischaemic conditions. The most conspicuous differences between mouse and human studies were observed in the recovery cycle and the response to hyperpolarization. Modelling showed that an increase in temperature in mouse axons could account for most of the differences in the recovery cycle. The modelling also suggested a larger hyperpolarization-activated conductance in mouse axons. The kinetics of this conductance appeared to be much slower raising the possibility that an additional or different hyperpolarization-activated cyclic-nucleotide gated (HCN) channel isoform underlies the accommodation to hyperpolarization in mouse axons. Given a possible difference in HCN isoforms, caution should be exercised in extrapolating from studies of mouse motor and sensory axons to human nerve disorders.

KEYWORDS

axonal excitability, motor axons, mouse, sensory axons, translational studies

1 | INTRODUCTION

Threshold-tracking techniques involving human motor and sensory nerves have become a valuable tool for understanding peripheral nerve function and underlying axonal membrane properties, supplementing conventional electrophysiological methods.[1,2] The availability of an automated sequence of multiple excitability tests[3,4] has greatly facilitated the clinical applicability of nerve excitability tests and has been successfully utilised to study the pathophysiology of multiple neurological disease[5–13] and the effects of therapy.[14,15]

Nerve excitability techniques have been adapted to in vivo and in vitro recordings in animal models.[16–24] The further development of a complete mouse model of motor and sensory excitability is warranted because the underlying molecular mechanisms and ion-channel regulation might be distinct in motor and sensory axons. Indeed, nerve excitability properties of human sensory nerve are distinct from those of human motor nerves. For example, compared to motor axons

Abbreviations: CMAP, compound muscle action potential; HCN, hyperpolarization-activated cyclic-nucleotide gated channels; I_h, hyperpolarization-activated current; IV, current-threshold relationship, the threshold-tracking analogue of current-voltage plots; RRP, relative refractory period; SDTC, strength-duration time constant; SNAP, sensory nerve action potential; TE, threshold electrotonus; TEd (10-20 milliseconds) (%), TEd (90-100 milliseconds) (%), threshold electrotonus measured 10-20 milliseconds and 90-100 milliseconds after the onset of a 40% depolarizing current, respectively; TEh (10-20 milliseconds) (%), TEh (90-100 milliseconds) (%), threshold electrotonus measured 10-20 milliseconds and 90-100 milliseconds after the onset of a 40% hyperpolarizing current, respectively

sensory axons have a lower stimulus-response slope, longer strength-duration time constant (SDTC), lower rheobase, less superexcitability and refractoriness during recovery cycle, different membrane potential, and different accommodative responses to polarisation.[25–27] In addition, the pathophysiological mechanisms that underlie axonal membrane changes in human peripheral nerve disorders are imperfectly understood, and widely used mouse models can contribute greatly to advancing the study of human conditions.

The excitability of motor axons has been explored in the caudal, sciatic and tibial nerves in healthy and diseased mice,[17,23,28,29] but there are limited data on sensory nerve excitability in mice. Orthodromic sensory nerve action potentials (SNAPs) in the mouse tail have been recorded in vivo[28,30,31] to stimulation at the distal segment of the tail, recording proximally. However, orthodromic motor and sensory recordings measure axonal properties at different sites and use different orientations of the stimulating electrodes (which affects measures such as the SDTC). Because nerve excitability studies assess the properties at the site of stimulation, the precise site of stimulation (ie, proximal/distal) could be important in dying-back neuropathies affecting peripheral nerves.

Accordingly, the present study describes a novel experimental protocol to enable study of SNAPs and compound muscle action potentials (CMAPs) from the same stimulation site at the base of the tail, thereby allowing the comparative assessment of the excitability of motor and sensory axons. Using this technique in mature C57BL/6J mice, we were able to discriminate between SNAPs, measured directly from the caudal nerve and CMAPs, recorded from tail muscle. These recordings were used to create a mathematical model of the excitability of mouse caudal nerve. In addition, to determine whether this model can be used as a tool to study human conditions, we compared the properties of mouse and human motor and sensory axons. As such, we present the first comprehensive mathematical model of the properties of sensory and motor axons recorded from the same site in mice, and use these models to clarify the differences between the peripheral nerve axons of mice and humans.

2 | METHODS

2.1 | Animals

Mature C57BL/6J mice (14 male and 19 female; Animal Resource Centre, Canning Vale, WA, Australia) aged 17 to 20 weeks were used for nerve excitability recordings apart from ischaemia studies. Animals were group-housed in sterile, individually ventilated cages and given ad libitum access to chow and water. A 12:12 hour light/dark cycle was maintained and housing was kept at a constant room temperature and humidity level. Mice were anaesthetised using 2% isoflurane and placed on a heat mat, which was adjusted to maintain a core body temperature close to 37°C, as measured by a rectal thermistor probe. All experiments were approved by the Animal Care and Ethics Committee of the University of New South Wales.

2.2 | Recordings of compound muscle and sensory nerve action potential in the mouse

The technique used to record orthodromic CMAPs in the mouse tail has been previously described.[17] Disposable non-polarizable Ag/AgCl ring electrodes (The Electrode Store; Buckley, Washington) were used for stimulation and grounding. The cathode was wrapped around the base of the tail and the anode around the ankle. Platinum needle electrodes (Natus; San Carlos, California) were used to record CMAPs, with the active electrode inserted into the tail muscle 20 to 30 mm distal to the cathode. To record antidromic SNAPs, the active electrode was inserted in the tail skin 65 to 70 mm distal to the cathode to record from the caudal nerves. In both cases the reference electrode was inserted 8 mm distal to the recording electrode and a ground electrode was placed between the stimulating and recording electrodes. The setup for recording CMAPs and SNAPs is illustrated in Figure 1A,C, respectively, and representative waveforms of CMAP and SNAP are depicted in Figure 1B,D, respectively. CMAP and SNAP waveforms were amplified (×100 for motor; ×10 k for sensory) and bandpass-filtered (3 Hz-3 kHz) using an isolated amplifier (D440-2 Digitimer Ltd; Welwyn Garden City, UK). The amplified signals had electrical interference from the power supply removed using a 50/60 Hz noise eliminator (HumBug; Quest Scientific; North Vancouver, BC, Canada) and were then digitised with a 16-bit data acquisition system (USB-6251; National instruments; Austin, Texas). Stimulation was delivered by an isolated stimulator (Model 2200 Analog Stimulus Isolator; A-M systems; Carlsborg, Washington).

2.3 | Ischaemia protocol in the mouse tail

Ischaemia was used as an experimental manoeuvre to test the comparability of mouse tail excitability to previously reported human studies. In separate recordings ischaemia was performed on additional cohorts of male mice (motor, $n = 9$, 32 ± 1.3 weeks; sensory, $n = 8$, 28.9 ± 2.3 weeks). Following anaesthesia, focal ischaemia was transiently induced at the base of the tail by mild constriction using elastic bands around the tail proximal to the site of stimulation. Nerve excitability testing was then performed on the tail, using the protocols described below. To track the post-ischaemic recovery phase, the constriction was removed, and nerve excitability testing was undertaken immediately afterwards using the same electrode setup as that used during the ischaemic phase. Each animal was subjected to either sensory or motor excitability testing in the ischaemic and post-ischaemic phases in order to reduce anaesthetic exposure and to minimise trauma that might be caused by the constriction.

2.4 | Human subjects

Recordings of the excitability of human motor and sensory axons were obtained from healthy control volunteers who provided consent prior to commencement of the study and were not taking medications with known neurological effects (motor, 9M/13F, age 38.4 ± 2.5 years; sensory, 10M/5F, age 47 ± 3.9 years). The study conformed to the requirements of the Declaration of Helsinki and was approved by the Human Research Ethics Committee of the University of Sydney.

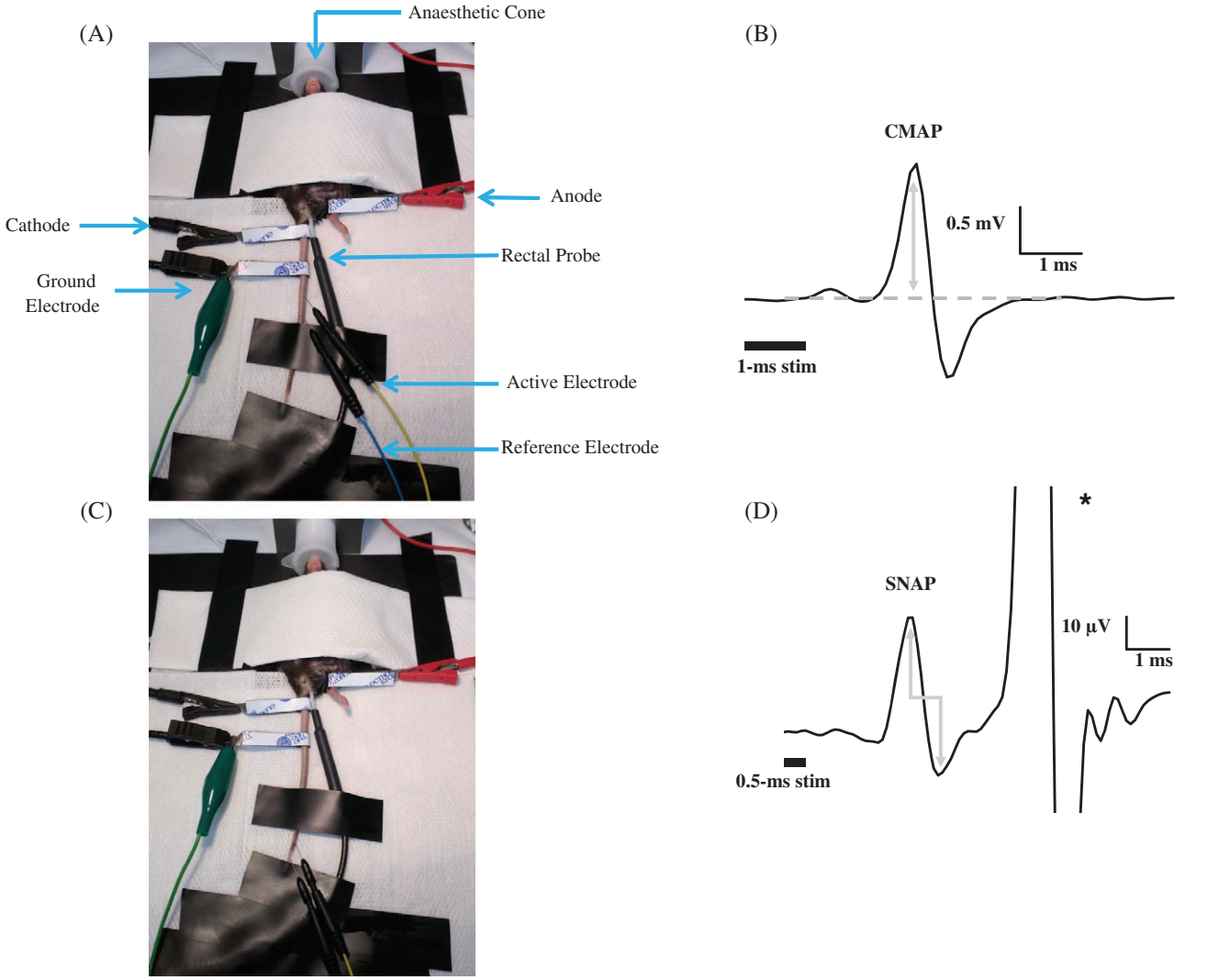

FIGURE 1 Schematic diagram of method for recording of compound muscle and sensory nerve action potentials (SNAPs) for the caudal nerve of the mouse tail. Recording arrangement, showing positions of nonpolarizable stimulation electrodes and needle electrodes for compound muscle (A) and sensory (C) action potentials. Compound muscle action potentials (CMAPs) (B) and SNAPs (D) recorded from the same site of stimulation at different levels of stimulus current. Grey arrows indicate the measurements (baseline to peak for CMAP; peak to peak for SNAP). The asterisk in (D) indicates a low-level CMAP that appeared when the SNAP was close to maximal

2.5 | Human compound muscle and sensory nerve action potential recordings

Axonal excitability recordings were obtained from the median nerve at the wrist in human subjects using disposable ECG-type Ag/AgCl electrodes. For motor studies a recording electrode was placed over the muscle belly of abductor pollicis brevis (APB) with the reference electrode fixed to the proximal phalanx of digit one and the ground electrode on the palm. For sensory studies disposable Ag/AgCl ring electrodes were used with one electrode placed as proximally as possible on the proximal phalanx of digit two and the reference 4 cm distally.[32] For the sensory studies the ground electrode was placed on the dorsal aspect of the hand. Recordings were amplified using a low-noise purpose built amplifier[33] (×250 for motor; ×10 k for sensory), and mains frequency contamination of the signal was again removed using a Humbug 50/60 Hz noise eliminator. Stimulation was delivered through surface electrodes over the median nerve at the wrist and 10 cm proximally, lateral and away from the course of the median nerve, using an isolated constant-current stimulator (DS5; Digitimer Ltd, Welwyn Garden City, UK). Temperature was monitored and kept constant to avoid temperature-induced changes in excitability.[34,35]

2.6 | Nerve excitability protocols

The QtracS threshold tracking software (©Institute of Neurology, UCL, London, UK) was used to control stimulation and data acquisition for both animal and human studies. Multiple excitability measurements were made with the TRONDNF protocol. Initially, the stimulus was manually set to a supramaximal level, following which the computer generated a stimulus-response relationship by progressively decreasing stimulus strength in 2% steps. For both motor and sensory recordings, the amplitude of the target response was set to be 40% of the amplitude of the maximal response, corresponding to the steepest phase of the stimulus-response curve. The current required to produce the target potential is termed the "threshold," and was tracked

using a 1-millisecond wide test stimulus for motor axons and 0.5-millisecond wide test stimulus for sensory axons.[3,4] For mouse sensory recordings, the "small sensory option" in the software was used for additional averaging.

2.7 | Strength-duration properties

The SDTC and rheobase were estimated by plotting the threshold stimulus charge in microcoulombs against stimulus duration in milliseconds for test stimuli of five different durations (0.2, 0.4, 0.6, 0.8, and 1 millisecond for motor recordings; 0.1, 0.2, 0.3, 0.4, and 0.5 millisecond for sensory), and determining the X-intercept and slope of the curve, respectively.[27,36]

2.8 | Threshold electrotonus

Threshold electrotonus (TE) measures the change in threshold before, during and after long-lasting sub-threshold polarisation. In this study, the response to polarisation was studied using the conventional TE protocol with depolarizing currents (20% and 40% of the control threshold) and hyperpolarizing currents (−20% and −40%). The response to hyperpolarization was clarified further using an extended protocol with longer and stronger hyperpolarizing currents: −70% of the control threshold for 200 milliseconds and −100% for 300 milliseconds.[25,37] Derived parameters associated with TE are referred to as follows: TEd, TEh refer to depolarizing and hyperpolarizing threshold electrotonus; the measurement interval was then appended, for example, TEd (10-20 milliseconds) refers to the average threshold reduction recorded between 10 and 20 milliseconds following the onset of a sub-threshold depolarizing current (+40% of the control threshold). Similarly, in the −40% threshold electrotonus curves the measurement TEh (90-100 milliseconds) corresponds to the threshold reduction at the end of a 100-millisecond long hyperpolarizing current. For −70% and −100% hyperpolarizing threshold electrotonus, TEh peak refers to the maximum increase in threshold and S3 is a measure of accommodation.

2.9 | Current-threshold relationship

The current-threshold (IV) relationship was recorded by measuring the threshold for the target potential at the end of a 200-millisecond polarising current. The strength of the polarising current was adjusted in 10% steps from +50% of the control threshold (depolarizing) to −100% of control threshold (hyperpolarizing).

2.10 | Recovery cycle

The recovery cycles of motor and sensory axons were recorded by measuring the threshold for the target potential following a supramaximal conditioning stimulus at 18 different conditioning-test intervals from 2 to 200 milliseconds. To define better the recovery cycle in mouse axons additional conditioning-test intervals were recorded namely: 1.5 and 1.3 milliseconds for motor axons; and 1.6 and 1.3 milliseconds for sensory axons.

At short conditioning-test intervals (<30 milliseconds for motor and <15 milliseconds for sensory axons), measurements of the conditioned response were made after subtraction of the response generated by the conditioning stimulus alone. In some sensory recordings, the CMAP occurred a few milliseconds after the sensory potential resulting in contamination of the SNAP for conditioning-test intervals less than about 5 milliseconds. In such cases, the conditioning stimulus was reduced from 170% to 150% at short intervals to minimise contamination of the recording by the CMAP.

2.11 | Mathematical modelling

A mathematical model of the excitability of mouse motor and sensory axons was developed based on the "Bostock" model of a human motor axon, as extended by Howells et al.[25] Briefly, the "Bostock" model is based on the excitability of a single node of Ranvier coupled to a single internode via axo-glial pathways, through and under the myelin sheath.[38] Voltage-gated ion channels and leak currents are modelled at the node and internode as follows: at the node, fast and persistent Na^+ currents, fast and slow K^+ currents, "leak" and Na^+/K^+ pump currents; on the internode, fast and slow K^+ currents, "leak" and Na^+/K^+ pump currents and the hyperpolarization-activated current I_h. A complete description of the mathematical model is included in the Appendix.

The model parameters were optimised using the fitting algorithm MEMFIT incorporated in the QtracP software (© Institute of Neurology, UCL, London, UK).[39] The MEMFIT algorithm reduces the discrepancy between the model and group data by varying selected model parameters (eg, channel expression, channel gating) until no further reduction in discrepancy is possible.

2.12 | Statistical analyses

Statistical analyses were performed using unpaired Student's *t* tests. *P*-values were corrected for multiple comparisons using the Holm-Bonferroni sequential correction.[40] The level of significance was set at $P < 0.05$ in all cases. All data are expressed as means ± SEM, except where the data were log-normally distributed in which case they are shown as geometric mean ×/÷ geometric SEM (as a factor).

3 | RESULTS

The properties of caudal sensory and motor axons were determined for the tails of both male and female mice. The core temperature of the mice was maintained at a mean of 37.2°C ± 0.01°C using a heat pad. A typical recording took less than 15 minutes for preparation, 12 minutes for motor recordings, and 23 minutes for sensory recordings. A combined recording was generally complete in 45 minutes, and all animals recovered normally from anaesthesia with no adverse events.

Axonal excitability recordings were similar in male and female mice: the only difference was in the response to long-lasting hyperpolarization (Figure 2). Male mice appeared to have faster activation of inwardly rectifying accommodative conductances than females. The difference in accommodation grew with stronger hyperpolarization and was significant in sensory axons (Table 1). A similar trend was apparent in motor axons, although not significant.

Because the excitability data were homogeneous in all other respects, the male and female data were combined for further analysis. Differences between male and female mice in accommodation to hyperpolarization will be addressed later in sections 3 and 4.

3.1 | Differences between mouse motor and sensory axons

Much as is the case with human recordings, the threshold for half-maximal activation and rheobase were lower in mouse sensory than mouse motor axons ($P < 0.009$ and 1.9×10^{-4}, respectively), and SDTC was significantly longer ($P = 3.4 \times 10^{-8}$; Table 2).

The relative refractory period was shorter and sub-excitability less in mouse sensory axons than motor ($P = 4.5 \times 10^{-7}$, $P < 0.04$, respectively; Table 2; Figure 3E,F). Superexcitability was not significantly different between mouse sensory and motor axons (Table 2; Figure 3E,F).

In human studies, the hyperpolarization-activated current I_h has been identified as a key difference underlying the excitability of motor and sensory axons.[25] In addition to the standard protocol for measuring the response to hyperpolarization (Figure 3A-D; Table 2), an extended protocol with longer and stronger hyperpolarizing currents was employed to gain a better understanding of the voltage dependence and kinetics of the underlying hyperpolarization-activated cyclic-nucleotide gated (HCN) channels in mouse axons (Figure 4). Meaningful comparisons of TE and the current-threshold relationship cannot be made directly between motor and sensory axons because the strength of conditioning currents are based on test pulses of different widths. However, the biophysical properties underlying these measures can be explored reliably using mathematical modelling, allowing differences between sensory and motor axons to be identified (see Reference 25).

TABLE 1 Differences between sensory axons in male and female mice in response to long-lasting hyperpolarization

Parameter	Male	Female	*P*-value
TEh (10-20 ms)	−85.1 ± 1.5	−93.0 ± 1.0	0.0019
TEh (90-100%)	−128.9 ± 6.9	−153.6 ± 3.2	0.016
TEh (overshoot)	8.2 ± 0.7	9.3 ± 0.5	1
TEh (peak, −70%)	−253.1 ± 9.3	−291 ± 4.2	0.0043
S3 (−70%)	86.7 ± 4.8	120.2 ± 3.1	3.7×10^{-5}
TEh (peak, −100%)	−339.7 ± 7.4	−392.9 ± 7.7	0.0054
S3 (−100%)	118.2 ± 3.7	163.4 ± 6.9	0.0018
Hyperpol. IV slope	0.55 ± 0.02	0.52 ± 0.02	1

Data are expressed as mean ± SEM. *P*-values corrected for multiple comparisons using the Holm-Bonferroni method.

3.2 | Comparison with human recordings

The nerve excitability waveforms recorded from the sensory axons of mouse caudal nerve were qualitatively similar to those recorded from

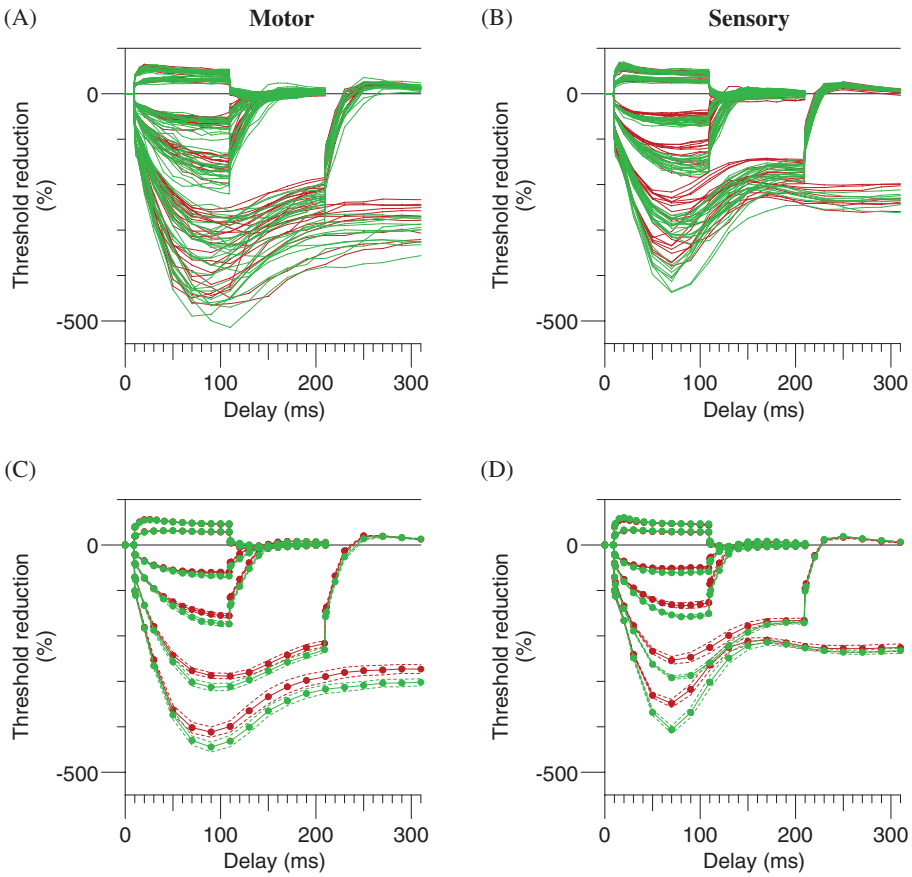

FIGURE 2 Excitability differences in male and female mouse motor and sensory axons. Recordings from male and female axons shown in red and green, respectively. Superimposed excitability waveforms for threshold electrotonus presented for motor (A) and sensory axons (B). Mean excitability waveforms for motor (C) and sensory axons (D). Solid and dotted lines signify mean ± SEM

TABLE 2 Comparison of excitability of motor and sensory axons in mouse and humans

	Mouse		Human	
Parameter	**Motor**	**Sensory**	**Motor**	**Sensory**
Stimulus-response				
Threshold for 50% response (mA)	0.28 ×/÷ 1.07	0.21 ×/÷ 1.06	4.3 ×/÷ 1.09	3.5 ×/÷ 1.09
SDTC (μs)	0.16 ± 0.01	0.27 ± 0.01	0.45 ± 0.02	0.60 ± 0.03
Rheobase (mA)	0.22 ×/÷ 1.07	0.14 ×/÷ 1.07	2.8 ×/÷ 1.09	1.5 ×/÷ 1.10
Current-threshold				
Resting IV slope	0.57 ± 0.02	0.53 ± 0.02	0.56 ± 0.01	0.55 ± 0.02
Hyperpolarizing IV slope	0.46 ± 0.02	0.53 ± 0.01	0.36 ± 0.01	0.35 ± 0.02
Minimum IV slope	0.26 ± 0.01	0.33 ± 0.01	0.25 ± 0.01	0.24 ± 0.01
Threshold electrotonus (±40%)				
TEd (10-20 ms) (%)	55.3 ± 0.8	56.5 ± 0.8	68.1 ± 0.9	63.1 ± 0.5
TEd (90-100 ms) (%)	46.3 ± 0.8	45.7 ± 0.6	46.2 ± 0.7	49.2 ± 1.2
TEd undershoot (%)	−8.0 ± 0.7	−9.2 ± 0.7	−17.8 ± 0.9	−20.2 ± 1.0
TEh (10-20 ms) (%)	−84.3 ± 2.1	−89.9 ± 1.1	−77.0 ± 1.4	−83.8 ± 1.8
TEh (90-100 ms) (%)	−165.8 ± 4.0	−144.1 ± 3.9	−125.1 ± 5.7	−133.6 ± 3.7
TEh overshoot (%)	8.7 ± 0.7	8.8 ± 0.4	13.9 ± 1	15.4 ± 1.1
Threshold electrotonus (−70% and −100%)				
TEh peak (−70%)	−306.8 ± 5.7	−276.4 ± 5.5	—	—
S3 (−70%)	76.5 ± 5.0	107.2 ± 4.0	—	—
TEh peak (−100%)	−430.4 ± 8.3	−366.3 ± 9.0	—	—
S3 (−100%)	141.8 ± 4.9	140.8 ± 7.3	—	—
Recovery cycle				
RRP (ms)	2.28 ×/÷ 1.02	1.74 ×/÷ 1.04	3.0 ×/÷ 1.02	3.2 ×/÷ 1.05
Superexcitability (%)	−13.2 ± 0.60	−15.0 ± 0.9	−22.6 ± 1.5	−18.9 ± 1.9
Subexcitability (%)	3.7 ± 0.4	2.6 ± 0.3	14.8 ± 1.1	9.6 ± 0.5

Abbreviations: SDTC, strength-duration time constant; TEd and TEh, depolarizing and hyperpolarizing threshold electrotonus; RRP, relative refractory period. The data are expressed as mean ± SEM, except where the data are log-normally distributed in which case they are shown as geometric mean ×/÷ geometric SEM (expressed as a factor).

human sensory axons in the median nerve. Despite these similarities, differences in the excitability of mouse and human axons are evident in all aspects of axonal excitability (Figure 5, Table 2). In part, such differences are due to different recording conditions, and therefore caution is warranted when making direct comparisons between the excitability of human and mouse axons. Nevertheless the mechanisms underlying the excitability of human and mouse recordings are common, and comparisons can be made with the assistance of a mathematical model, which is discussed later.

During TE, there was a smaller threshold change in response to depolarizing currents and reduced undershoot when the current ended in recordings from mouse sensory nerve (Figure 5B). Hyperpolarization for 100 milliseconds was insufficient to reveal differences in inward rectification (lower half of Figure 5B), but greater inward rectification was apparent in mouse axons with the longer currents used for the IV and IV slope plots (Figure 5F,H).

Mouse and human motor excitability waveforms were also qualitatively similar and the findings in the present study are consistent with the mouse data of Boërio et al.[17,41] As was the case with sensory axons, there was a lesser threshold change during depolarizing TE in mouse motor axons and, on termination of the current, the threshold undershoot was smaller (Figure 5A). The response to hyperpolarization was different in motor axons, with less accommodation to moderate hyperpolarization in the mouse (bottom of Figure 5A). However, with stronger and longer hyperpolarization, mouse motor axons showed greater accommodation in the current-threshold relationship (Figure 5E,G), much as was the case with sensory axons.

The recovery cycle was flatter and earlier in mouse than in human axons (Figure 5C,D; Table 2). For both motor and sensory axons, the relative refractory period was shorter (motor, $P = 1.9 \times 10^{-10}$; sensory, $P = 6.1 \times 10^{-10}$). The amplitudes of superexcitability and subexcitability were smaller in mouse axons (superexcitability: motor [$P = 9.8 \times 10^{-8}$], sensory [$P = 0.06$]; subexcitability: motor [$P = 3.9 \times 10^{-13}$], sensory [$P = 3.5 \times 10^{-10}$]).

3.3 | Response to ischaemia

Qualitatively, the effect of ischaemia on the excitability of mouse axons in the present study was remarkably similar to that in published studies for human motor axons.[42] Motor and sensory axons were depolarized during ischaemia with reversion towards resting values after release of ischaemia (Figure 6). The "fanned-in" appearance of TE, the steeper resting I/V slope and recovery cycle shifted up and to the right are expected with axonal depolarization during ischaemia, much as has been observed in human axons.[42]

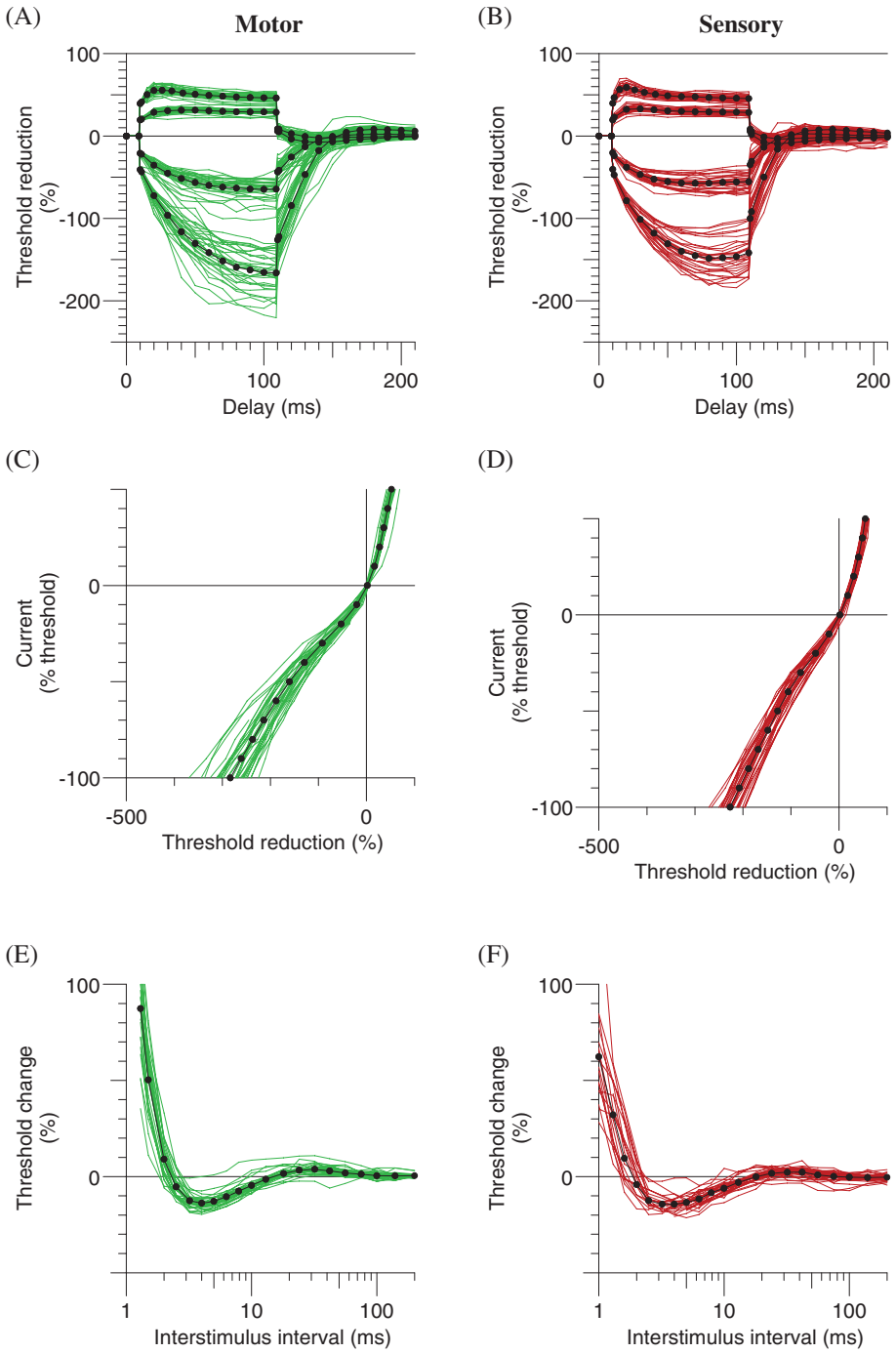

FIGURE 3 Excitability properties of mouse caudal motor and sensory axons. Superimposed excitability waveforms presented for motor (green, n = 33) and sensory (red, n = 31) axons, and mean excitability waveforms presented in black. Panels A and B depict threshold electrotonus for sub-threshold polarising currents ±20% and ±40% of threshold for motor and sensory axons, respectively. Panels *C* and *D* show the current-threshold (IV) relationship for motor and sensory axons, respectively. Panels *E* and *F* represent the recovery cycle following supramaximal conditioning stimulus for motor and sensory axons, respectively. Data for male and female mice are combined

3.4 | Modelling

As mentioned previously, direct comparisons are difficult to make between the excitability of human and mouse axons, particularly under different recording conditions. To tackle this problem, we used a mathematical model of axonal excitability to compare the active and passive properties underlying human and mouse excitability.

The "Bostock" model of excitability of human motor axons, as modified and extended to sensory axons by Howells et al,[25] was used as the basis for modelling the excitability of myelinated axons of mouse caudal nerve. No changes in the structure of the model were required, and the relationship between nodal and internodal compartments and the types of ion channels were the same in both models.[25] The strategy was to fit first the modified "Bostock" model of a human motor axon to the mouse motor data, and then to use that as the starting point to model the mouse sensory data. The MEMFIT function within the QtracP software was used to find the optimal model

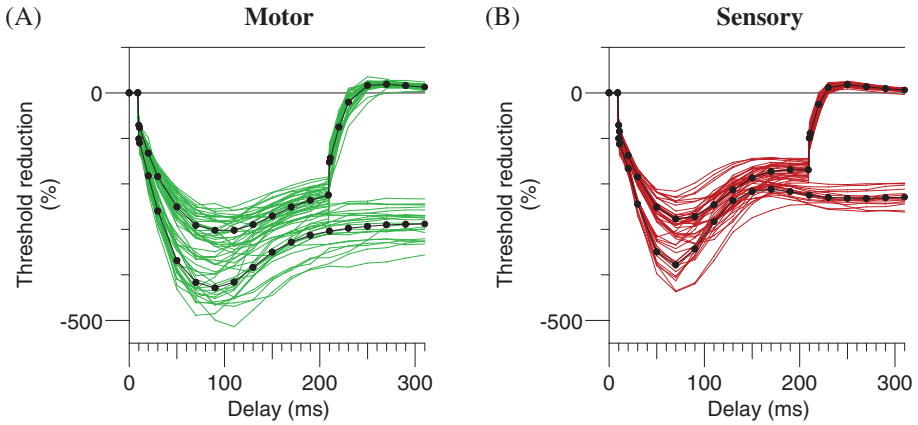

FIGURE 4 Extended hyperpolarising threshold electrotonus of mouse caudal motor and sensory axons. Superimposed extended excitability waveforms presented for motor and sensory axons (green and red lines, respectively), and mean excitability waveforms presented in black. Panels *A* and *B* depict threshold electrotonus for hyperpolarising currents −70% and −100% of threshold for motor and sensory axons, respectively. Data for male and female mice are combined

parameters applicable to mouse motor axons. The parameters underlying the difference in human motor axons and mouse motor and sensory axons are outlined in Table 3, and the modelled excitability measures are compared to the recorded data in Figure 7.

3.5 | Motor axons

For motor axons, the mouse model of a motor axon differed from the human model in the nodal capacitance, axonal temperature and expression of voltage-gated, "leak" and "Barrett-Barrett" conductances. The changes listed in the mouse motor column of Table 3 produced an excellent fit for the experimental data, accounting for 98.8% of the difference between the human motor model and the mouse motor data.

The modelling suggested a 5.9°C warmer axonal temperature in motor axons in the proximal caudal nerve of mice than in human median nerve. This increase in temperature alone could account for 77.7% of the overall difference between the human model and the mouse motor data (specifically: strength-duration properties, 68.6%; TE, 29.4%; recovery cycle, 99.4%; current-threshold relationship, 61.2%). In contrast with the findings of,[41] the modelling suggested that an increase in the permeability of Na^+ channels at the node would best describe the mouse excitability data. The modelling also suggested larger fast K^+ and smaller slow K^+ conductances in mouse motor axons. This would contribute to the smaller peak of depolarizing TE and the smaller undershoot when the polarising current ended.

The remaining difference between human and mouse motor recordings was a stronger but slower accommodative response to long-lasting hyperpolarization in mouse axons, and this could be reproduced by doubling the conductance (G_H) and halving the activation rate of HCN channels in the mouse model.

3.6 | Sensory axons

The mouse motor model was then applied to the mouse sensory data, and each parameter was allowed to vary to minimise the difference between the model and data. The key differences between the mouse motor and sensory models are shown in Table 3: a smaller nodal fast K^+ conductance (G_{KfN}) and a larger conductance, activated at a more hyperpolarized membrane potential, through HCN channels (G_H). These changes reduced the discrepancy between the mouse motor model and the mouse sensory data by 98.8%.

The changes in both mouse models resulted in a slightly more hyperpolarized resting membrane potential than in the human model, much as was reported for motor axons by Boërio et al.[41] The optimal mouse sensory model was more depolarized than the mouse motor model, but only by 0.5-mV, a difference that is less than previously reported for human axons (~4 mV).[25]

3.7 | Modelled differences between male and female mice

The only differences in the excitability of male and female mice were the responses to hyperpolarization in TE and the IV curves, findings that suggest a difference in the activation of the hyperpolarization-activated current, I_h, which passes through HCN channels. In keeping with this, the best single parameter reducing the discrepancy between the combined models and the male or female data was the activation rate of HCN channels (Aq). For the CMAP recordings, increasing the activation rate for the male recordings by 25% (more than that optimal for the whole mouse population) improved the discrepancy between the combined data and the male recordings by 16%, and decreasing it for the female recordings improved the discrepancy by 71%.

For the SNAP recordings the findings were similar with an increase in Aq of 19% in males and decrease of 16% in females, improving the model fits by 76% and 65%, respectively.

4 | DISCUSSION

This study presents a novel method for recording SNAPs in mouse tail axons, using the same site of stimulation as for motor axons. Using this technique, we have obtained normative excitability data for motor and sensory axons from the tails of mature male and female mice, and provide the first combined mathematical model of the excitability of

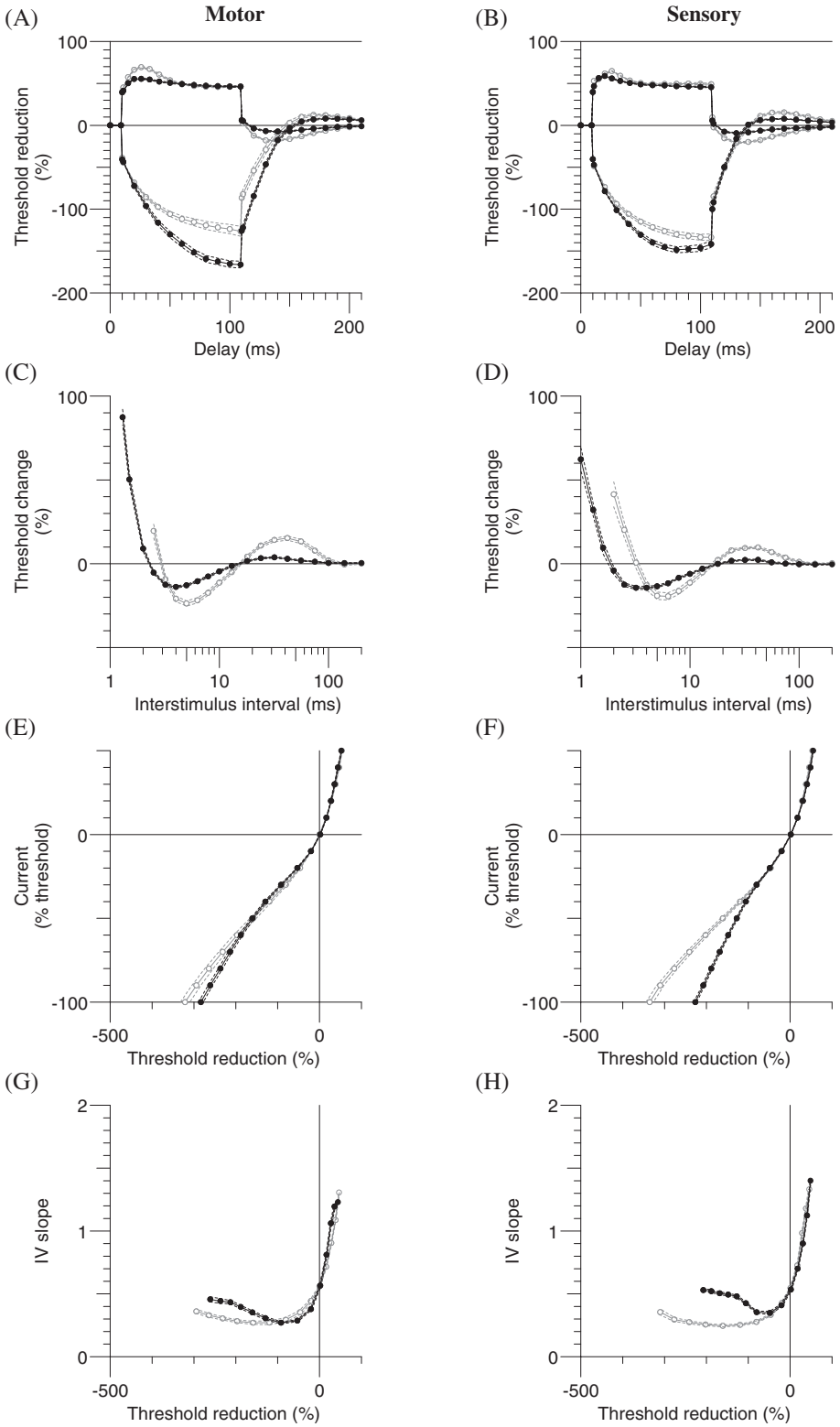

FIGURE 5 Excitability properties of mouse and human axons. Motor and sensory excitability waveforms presented as mean ± SEM mouse (black circles; motor = 33; sensory = 31) and human (clear circles; motor = 22; sensory = 15) waveforms. Panels *A* and *B* depict threshold electrotonus for sub-threshold polarising currents ±40% of threshold for motor and sensory axons, respectively. Panels *C* and *D* represent recovery cycle following supramaximal conditioning stimulus for motor and sensory axons, respectively. Panels *E* and *F* show the current-threshold (IV) relationship for motor and sensory axons, respectively. Panels *G* and *H* depict the IV slope for motor and sensory axons, respectively

mouse motor and sensory axons. We also compare the data for the mouse caudal nerve to those for the human median nerve, a prerequisite if mouse models are to be used in translational studies of human disease. Some of the differences between the way motor and sensory axons are measured in mouse and human studies preclude direct comparison of excitability waveforms (see section 3), such that modelling represents the only valid way to explore the biophysical basis of differences in the behaviour of the two modalities in the two species.

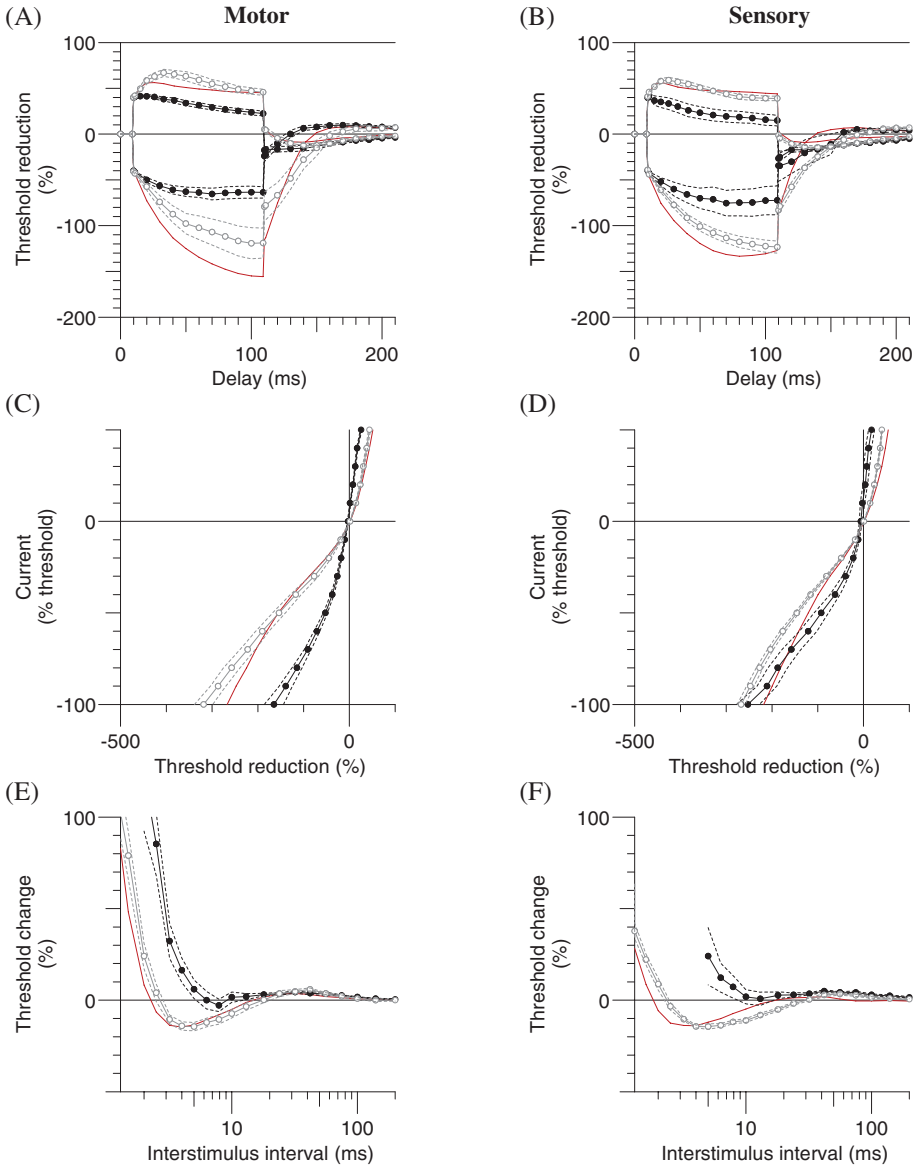

FIGURE 6 Excitability of mouse axons during and post-ischaemia. Motor (n = 9) and sensory (n = 8) excitability waveforms presented as mean ± SEM during ischaemia (filled black circles) and post-ischaemia (empty grey circles). Mean control recordings of male mice from Figure 2 are shown for comparison as red lines. Panels *A* and *B* depict threshold electrotonus for sub-threshold polarising currents ±40% of threshold for motor and sensory axons, respectively. Panels *C* and *D* show the current-threshold (IV) relationship for motor and sensory axons, respectively. Panels *E* and *F* represent recovery cycle following supramaximal conditioning stimulus for motor and sensory axons, respectively

4.1 | Comparison of mouse sensory and motor excitability

Our recordings of the excitability of mouse motor axons are comparable to the previously published data from mouse tail.[17,41] Our normative sensory data, however, differs from earlier recordings[28,30,31] which used an orthodromic technique, stimulating the distal tail and recording proximally. Recording SNAPs antidromically using proximal stimulation has many advantages, which will be discussed later.

The modelling suggested that the main differences between mouse sensory and motor axons are a reduced fast K^+ conductance and a larger, but slower conductance through HCN channels.

The only difference in excitability between male and female mice was a slightly faster activation of inwardly rectifying conductances in the caudal nerve of male mice. Studies in humans have not identified gender-based differences in nerve excitability.[43] However, there are no studies that have investigated gender-related differences in nerve excitability in mice. It is not practical to assess mouse nerve excitability in vivo without the use of anaesthetic, as used in our studies. Osaki et al[31] reported that isoflurane suppressed HCN channel activity in mice. It is possible that gender-based differences in excitability are due to an inherent difference in how male and female mice respond to the anaesthetic. Either way, the present results suggest that gender differences in mice may be an important consideration when constructing nerve excitability models of disease in mice.

4.2 | Comparison of mouse and human excitability

Qualitatively, the excitability waveforms for mouse caudal axons resemble those for the human median nerve. The same pattern of

TABLE 3 Modelled mouse motor and sensory parameters

		Human		Mouse	
Parameter	**Description**	**Sensory[a]**	**Motor**	**Motor**	**Sensory**
P_{NaN} ($cm^3\ s^{-1} \times 10^{-9}$)	Permeability of Na^+ channels at the node	4.35	4.35	8.45	8.45
P_{Nap} (%)	Percentage of Na^+ channels that are persistent	1.07	1.07	0.42	0.152
G_{KsN} (nS)	Max. conductance of slow K^+ channels at the node	29.1	56.7	40.3	40.3
G_{KsI} (nS)	Max. conductance of slow K^+ channels at the internode	1.74	0.57	1.16	1.16
G_{KfN} (nS)	Max. conductance of fast K^+ channels at the node	19.4	18.2	61	29
G_{KfI} (nS)	Max. conductance of fast K^+ channels at the internode	205	207	314	314
G_H (nS)	Max. conductance of I_h through HCN channels	4.1	2.95	6.55	26
A_q (ms^{-1})[b]	Activation rate of I_h through HCN channels	8.85×10^{-4}	8.85×10^{-4}	4.0×10^{-4}	3.65×10^{-4}
[A_q – male][b,c]				[5.0×10^{-4}]	[4.35×10^{-4}]
[A_q – female][b,c]				[3.35×10^{-4}]	[3.05×10^{-4}]
B_q (mV)	Membrane potential for half-maximal activation of I_h	−94.2	−107.3	−100.5	−108.9
G_{LkN} (nS)	Leak conductance at the node	1.69	1.97	0.89	0.89
G_{Lk} (nS)	Leak conductance at the internode	3.65	4	3.35	3.65
G_{BB} (nS)	Barrett-Barrett conductance	40.3	35.9	44	44
ENR (mV)	Nodal RMP (nodal pump current; nA)	−80.3 (−0.054)	−84.4 (−0.033)	−85.0 (−0.045)	−84.5 (−0.045)
EIR (mV)	Internodal RMP (internodal pump current; nA)	−81.3 (−0.0043)	−84.6 (−0.00786)	−85.5 (0.0193)	−85.0 (0.008)
Tabs (°K)	Temperature	304.8	304.8	310.7	310.7
CN (pF)	Nodal capacitance	1.4	1.4	0.5	0.5

[a] Human sensory parameters included for completeness.

[b] Activation rates specified at 20°C.

[c] Activation rates in brackets denote the best fit to the male/female differences in the mouse model.

accommodation to polarisation and change in excitability following activation occurs in the axons of mouse tail and the human median nerve. The underlying mechanisms of excitability are likely to be similar in mouse tail and human median nerve. In accordance with this view, the differences between these recordings could be explained without structural alteration of the mathematical model. The species differences were particularly prominent in the recovery cycle, where they were reminiscent of those seen with Na^+ channel blockade due to acute tetrodotoxin poisoning in humans.[7] The modelling, however, suggests that recording temperature was more likely to account for the difference in the recovery cycles of mouse and human subjects. This is consistent with the well-recognised thermoregulatory role and steep temperature decline along the mouse tail.[44–46]

In addition to an increased axonal temperature in the mouse tail, the present results indicate a greater fast K^+ conductance and the modelling suggested a greater Na^+ conductance. This contrasts with the findings of Boërio et al[41] who found that a lower sodium channel density explained most of the differences between mouse and human motor axons in their study. There are several differences between the present study and that of Boërio et al[41] that may explain the different conclusions. First, temperature was not considered in the earlier study, and this factor can have a profound effect on Na^+ currents. Second, the present study included the extended protocol which allows for more reliable modelling because it effectively reduces the number of degrees of freedom when exploring the model parameter space. Third, both motor and sensory axons were modelled better by an increase in temperature and Na^+ conductance.

The remaining difference was a larger, but slower and hyperpolarized conductance through HCN channels. The slower kinetics of this conductance in the mouse data raise the possibility that slower isoforms are responsible for or contribute to the inward rectification seen in the mouse tail. The HCN1, HCN2, and HCN3 isoforms have been detected in mouse dorsal root ganglion cells,[47] although the cellular expression of HCN isoforms in mouse peripheral nerve, or human nerve for that matter, remains unknown. The possibility that different HCN channels (whether "pure" homomeric or heteromeric combinations) underlie the accommodation to hyperpolarizing currents in mouse and human axons has important implications for translational studies of disease processes or ion channel modifiers that involve HCN channels.

It is unlikely that isoflurane is responsible for the difference in activation kinetics between mouse and human axons. Isoflurane is known to hyperpolarize the voltage activation of HCN1 channels, and to reduce the maximal activation of HCN2 channels.[48] Neither of these mechanisms would affect activation kinetics, and it is likely that the slower activation of I_h in the present study is underestimated as the mouse axonal temperature is estimated to be 6° warmer than in human median nerve studies.

Mouse motor and sensory axons behaved in a remarkably similar manner to human axons both during and after an ischaemic

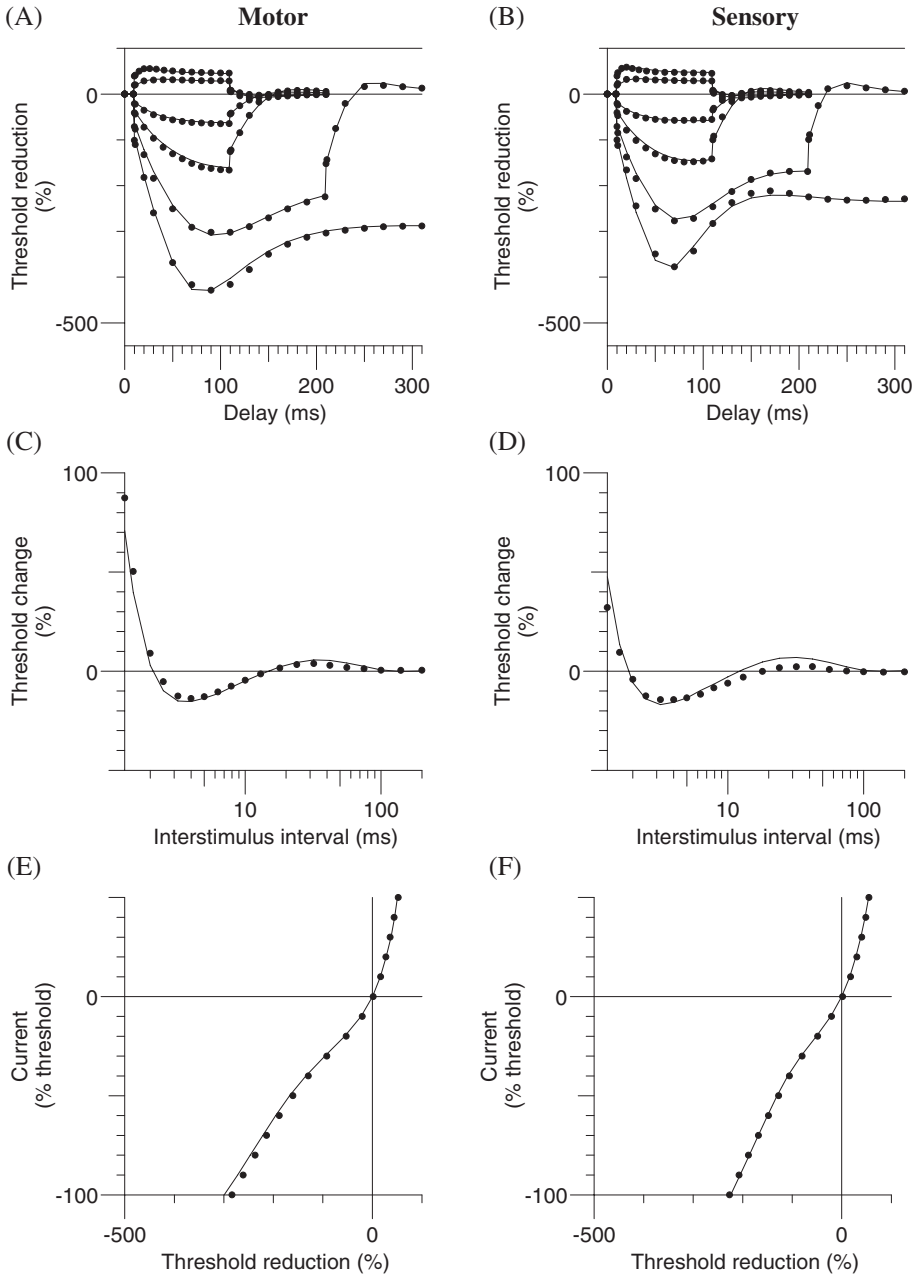

FIGURE 7 Modelled excitability of mouse motor and sensory axons. Experimentally recorded data represented as mean excitability waveforms (black circles) superimposed on the mathematically modelled waveforms (continuous black lines). Panels *A* and *B* represent mean and model threshold electrotonus for subthreshold polarising currents ±20% and ±40% of threshold; panels *C* and *D* represent mean and model recovery cycle following supramaximal conditioning stimulus; panels *E* and *F* represent mean and model current-threshold (IV) relationship; Motor and sensory waveforms are shown in the left- and right-hand columns, respectively

manoeuvre, further suggesting the utility of the mouse tail as a translational platform for understanding human disease and response to therapeutic intervention.

4.3 | Advantages of studying sensory and motor axons at the base of the mouse tail

The availability of transgenic mouse models allows for targeted knock-out studies, making the mouse an ideal choice for experimental modelling of peripheral neuropathy and neurodegenerative conditions such as ALS.[49–52] The excitability of sensory axons has been previously studied in mouse tail using an orthodromic recording setup with distal stimulation.[22,28,30]

However, studying sensory and motor axons at the same site at the base of the tail has some advantages.

First, this technique allows for separation of the SNAP and CMAP on latency grounds, thereby allowing the tracking of a pure sensory response. Given enough separation between the stimulating and recording electrodes, the SNAPs appear earlier than the CMAPs because of slower conduction in the motor nerve terminals and the synaptic delay at the neuromuscular junction. By careful positioning of the recording electrodes and measurement window, it is possible to record a maximal peak-to-peak SNAP without distortion due to

overlap with the low-level CMAP, a problem that has been documented in the much larger tail of rats.[19] To achieve adequate separation between SNAP and CMAP, we limited our study to mature animals with tail lengths greater than 6 cm. A further improvement in the recording yield was made by reducing the conditioning stimulus intensity from 170% to 150% of the control threshold. This represents a compromise between CMAP contamination and the maximal recordable refractoriness.

Second, studying both motor and sensory axons at the same site, at the base of the tail, will give comparable recording temperatures that are more stable and better correlated with core temperature rather than ambient temperature.

Third, our technique of recording SNAPs antidromically using the same site of stimulation as for orthodromic motor recordings allows a direct comparison of axonal properties in sensory and motor axons at the same level. The ability to study both motor and sensory axons at the same site of stimulation allows better comparisons in neuropathies that affect both sensory and motor axons. For neuropathies that selectively affect predominantly sensory or motor modalities, the other modality can be used as an internal control.

Last, mouse sensory studies that use an orthodromic montage for sensory recordings show a pattern of excitability that looks more "depolarized" than the recordings in the present study. There are two key differences in the recording arrangements. First, whereas the earlier studies used stainless steel needle electrodes for stimulation,[28,30,31] we used Ag/AgCl ring electrodes on the surface to minimise the risk of polarisation at the site of stimulation. This can be especially problematic when strong polarisation currents are used, such as for extended hyperpolarizing TE. Second, it is likely that there are differences in the excitability of sensory axons at proximal and distal sites. This would be consistent with our unpublished observations that the excitability of axons measured at the digit in human median nerve appear "depolarized" when compared to recordings made at the wrist.

In conclusion, the present study presents a number of novel unexpected findings for mouse axons. First, there seem to be differences between the axonal properties of male and female mice, involving particularly the activation rate of HCN channels. Second, human and mouse axons appear to differ in I_h, possibly because they express different HCN isoforms. These differences mean that prudence is required in using the mouse as a suitable model for human diseases.

Nevertheless, our study shows that minimally invasive threshold tracking of SNAPs and CMAPs is possible in the mouse tail, allowing multiple excitability parameters of motor and sensory axons to be easily studied and compared in vivo. The development of a comprehensive the mathematical model of sensory and motor axons in the mouse provides a much-needed tool for comparison with human excitability. This in vivo technique can be applied to transgenic mice and, provided that the above caveats are kept in mind (and in particular avoidance of direct comparisons of human and mouse excitability), the described technique is suitable for longitudinal studies using the same animals, thus enabling modelling of disease progression. The technique provides a translational platform for the development of new treatment interventions.

ACKNOWLEDGMENTS

This research was supported by the Cancer Institute NSW Translational Program Grant - "Chemotherapy-induced Peripheral Neuropathy: Assessment strategies, Treatment and Risk Factors" (ID # 14/TPG/1-05); and a program grant (#1037746) from the National Health and Medical Research Council of Australia (NHMRC). JH was supported by a Bill Gole MND Fellowship from the Motor Neurone Disease Research Institute of Australia.

Conflict of interest

P.M., J.M., S.P., J.L., G.M.-T., J.H. report no competing interests. M.K. serves as Editor-in-Chief of the *Journal of Neurology, Neurosurgery and Psychiatry*. D.B. serves as Editor-in-Chief of *Clinical Neurophysiology Practice*.

ORCID

Gila Moalem-Taylor http://orcid.org/0000-0003-3828-9527

REFERENCES

1. Bostock H, Cikurel K, Burke D. Threshold tracking techniques in the study of human peripheral nerve. *Muscle Nerve*. 1998;21:137-158.
2. Krishnan AV, Lin CS-Y, Park SB, Kiernan MC. Axonal ion channels from bench to bedside: a translational neuroscience perspective. *Prog Neurobiol*. 2009;89:288-313.
3. Kiernan MC, Burke D, Andersen KV, Bostock H. Multiple measures of axonal excitability: a new approach in clinical testing. *Muscle Nerve*. 2000;23:399-409.
4. Kiernan MC, Lin CS-Y, Andersen KV, Murray NM, Bostock H. Clinical evaluation of excitability measures in sensory nerve. *Muscle Nerve*. 2001;24:883-892.
5. Bae JS, Simon NG, Menon P, Vucic S, Kiernan MC. The puzzling case of hyperexcitability in amyotrophic lateral sclerosis. *J Clin Neurol*. 2013;9:65-74.
6. Heide R, Bostock H, Ventzel L, et al. Axonal excitability changes and acute symptoms of oxaliplatin treatment: in vivo evidence for slowed sodium channel inactivation. *Clin Neurophysiol*. 2018;129:694-706.
7. Kiernan MC, Isbister GK, Lin CS-Y, Burke D, Bostock H. Acute tetrodotoxin-induced neurotoxicity after ingestion of puffer fish. *Ann Neurol*. 2005;57:339-348.
8. Kiernan MC, Krishnan AV, Lin CS-Y, Burke D, Berkovic SF. Mutation in the Na+ channel subunit SCN1B produces paradoxical changes in peripheral nerve excitability. *Brain*. 2005;128:1841-1846.
9. Krishnan AV, Lin CS-Y, Kiernan MC. Activity-dependent excitability changes suggest Na+/K+ pump dysfunction in diabetic neuropathy. *Brain*. 2008;131:1209-1216.
10. Kuwabara S, Ogawara K, Sung JY, et al. Differences in membrane properties of axonal and demyelinating Guillain-Barre syndromes. *Ann Neurol*. 2002;52:180-187.
11. Nodera H, Bostock H, Kuwabara S, et al. Nerve excitability properties in Charcot-Marie-Tooth disease type 1A. *Brain*. 2004;127:203-211.
12. Tomlinson SE, Tan SV, Kullmann DM, et al. Nerve excitability studies characterize Kv1.1 fast potassium channel dysfunction in patients with episodic ataxia type 1. *Brain*. 2010;133:3530-3540.
13. Vucic S, Kiernan MC. Upregulation of persistent sodium conductances in familial ALS. *J Neurol Neurosurg Psychiatry*. 2010;81:222-227.
14. Lin CS-Y, Krishnan AV, Park SB, Kiernan MC. Modulatory effects on axonal function after intravenous immunoglobulin therapy in chronic inflammatory demyelinating polyneuropathy. *Arch Neurol*. 2011;68:862-869.
15. Vucic S, Lin CS-Y, Cheah BC, et al. Riluzole exerts central and peripheral modulating effects in amyotrophic lateral sclerosis. *Brain*. 2013;136:1361-1370.

16. Arnold R, Moldovan M, Rosberg MR, Krishnan AV, Morris R, Krarup C. Nerve excitability in the rat forelimb: a technique to improve translational utility. *J Neurosci Methods*. 2017;275:19-24.
17. Boërio D, Greensmith L, Bostock H. Excitability properties of motor axons in the maturing mouse. *J Peripher Nerv Syst*. 2009;14:45-53.
18. Campero M, Ezquer M, Ezquer F. Nerve excitability and structural changes in myelinated axons from diabetic mice. *Exp Clin Endocrinol Diabetes*. 2015;123:485-491.
19. George A, Bostock H. Multiple measures of axonal excitability in peripheral sensory nerves: an in vivo rat model. *Muscle Nerve*. 2007;36:628-636.
20. Maurer K, Bostock H, Koltzenburg M. A rat in vitro model for the measurement of multiple excitability properties of cutaneous axons. *Clin Neurophysiol*. 2007;118:2404-2412.
21. Moldovan M, Alvarez S, Krarup C. Motor axon excitability during Wallerian degeneration. *Brain*. 2009;132:511-523.
22. Nodera H, Spieker A, Sung M, Rutkove S. Neuroprotective effects of Kv7 channel agonist, retigabine, for cisplatin-induced peripheral neuropathy. *Neurosci Lett*. 2011;505:223-227.
23. Sawai S, Kanai K, Nakata M, et al. Changes in excitability properties associated with axonal regeneration in human neuropathy and mouse Wallerian degeneration. *Clin Neurophysiol*. 2008;119:1097-1105.
24. Yang Q, Kaji R, Hirota N, et al. Effect of maturation on nerve excitability in an experimental model of threshold electrotonus. *Muscle Nerve*. 2000;23:498-506.
25. Howells J, Trevillion L, Bostock H, Burke D. The voltage dependence of I(h) in human myelinated axons. *J Physiol*. 2012;590:1625-1640.
26. Kiernan MC, Mogyoros I, Burke D. Differences in the recovery of excitability in sensory and motor axons of human median nerve. *Brain*. 1996;119:1099-1105.
27. Mogyoros I, Kiernan MC, Burke D. Strength-duration properties of human peripheral nerve. *Brain*. 1996;119:439-447.
28. Nodera H, Rutkove SB. Accommodation to hyperpolarizing currents: differences between motor and sensory nerves in mice. *Neurosci Lett*. 2012;518:111-116.
29. Nodera H, Rutkove SB. Changes of the peripheral nerve excitability in vivo induced by the persistent Na+ current blocker ranolazine. *Neurosci Lett*. 2012;518:36-40.
30. Banzrai C, Nodera H, Higashi S, et al. Age-dependent effects on sensory axonal excitability in normal mice. *Neurosci Lett*. 2016;611:81-87.
31. Osaki Y, Nodera H, Banzrai C, et al. Effects of anesthetic agents on in vivo axonal HCN current in normal mice. *Clin Neurophysiol*. 2015;126:2033-2039.
32. Eduardo E, Burke D. The optimal recording electrode configuration for compound sensory action potentials. *J Neurol Neurosurg Psychiatry*. 1988;51:684-687.
33. Howells J, Bostock H, Park SB, Kiernan MC, Burke D. Tracking small sensory nerve action potentials in human axonal excitability studies. *J Neurosci Methods*. 2018;298:45-53.
34. Burke D, Mogyoros I, Vagg R, Kiernan MC. Temperature dependence of excitability indices of human cutaneous afferents. *Muscle Nerve*. 1999;22:51-60.
35. Kiernan MC, Cikurel K, Bostock H. Effects of temperature on the excitability properties of human motor axons. *Brain*. 2001;124:816-825.
36. Bostock H. The strength-duration relationship for excitation of myelinated nerve: computed dependence on membrane parameters. *J Physiol*. 1983;341:59-74.
37. Tomlinson S, Burke D, Hanna M, Koltzenburg M, Bostock H. In vivo assessment of HCN channel current (I(h)) in human motor axons. *Muscle Nerve*. 2010;41:247-256.
38. Barrett EF, Barrett JN. Intracellular recording from vertebrate myelinated axons: mechanism of the depolarizing afterpotential. *J Physiol*. 1982;323:117-144.
39. Bostock H. MEMFIT: a computer program to aid interpretation of multiple excitability measurements on human motor axons. *Clin Neurophysiol*. 2006;117:S85.
40. Holm S. A simple sequentially rejective multiple test procedure. *Scand J Stat*. 1979;6:65-70.
41. Boërio D, Greensmith L, Bostock H. A model of mouse motor nerve excitability and the effects of polarizing currents. *J Peripher Nerv Syst*. 2011;16:322-333.
42. Kiernan MC, Bostock H. Effects of membrane polarization and ischaemia on the excitability properties of human motor axons. *Brain*. 2000;123:2542-2551.
43. McHugh JC, Reilly RB, Connolly S. Examining the effects of age, sex, and body mass index on normative median motor nerve excitability measurements. *Clin Neurophysiol*. 2011;122:2081-2088.
44. Al-Hilli F, Wright EA. The effects of changes in the environmental temperature on the growth of tail bones in the mouse. *Br J Exp Pathol*. 1983;64:34-42.
45. Gordon CJ. Thermal physiology of laboratory mice: defining thermoneutrality. *J Therm Biol*. 2012;37:654-685.
46. Gordon CJ. The mouse thermoregulatory system: its impact on translating biomedical data to humans. *Physiol Behav*. 2017;179:55-66.
47. Moosmang S, Stieber J, Zong X, Biel M, Hofmann F, Ludwig A. Cellular expression and functional characterization of four hyperpolarization-activated pacemaker channels in cardiac and neuronal tissues. *Eur J Biochem*. 2001;268:1646-1652.
48. Chen X, Shu S, Kennedy DP, Willcox SC, Bayliss DA. Subunit-specific effects of isoflurane on neuronal Ih in HCN1 knockout mice. *J Neurophysiol*. 2009;101:129-140.
49. Boërio D, Kalmar B, Greensmith L, Bostock H. Excitability properties of mouse motor axons in the mutant SOD1(G93A) model of amyotrophic lateral sclerosis. *Muscle Nerve*. 2010;41:774-784.
50. Leandri M, Ghignotti M, Emionite L, Leandri S, Cilli M. Electrophysiological features of the mouse tail nerves and their changes in chemotherapy induced peripheral neuropathy (CIPN). *J Neurosci Methods*. 2012;209:403-409.
51. Makker PG, Duffy SS, Lees JG, et al. Characterisation of immune and neuroinflammatory changes associated with chemotherapy-induced peripheral neuropathy. *PLoS One*. 2017;12:e0170814.
52. Sullivan KA, Hayes JM, Wiggin TD, et al. Mouse models of diabetic neuropathy. *Neurobiol Dis*. 2007;28:276-285.

How to cite this article: Makker PGS, Matamala JM, Park SB, et al. A unified model of the excitability of mouse sensory and motor axons. *J Peripher Nerv Syst*. 2018;23:159–173. https://doi.org/10.1111/jns.12278

APPENDIX A: "BOSTOCK" MODEL OF A MYELINATED AXON. (ADAPTED FROM HOWELLS ET AL., 2012)[25]

Membrane potential:

$$\frac{dE}{dt} = -\frac{(I_{Na} + I_{Kf} + I_{Ks} + I_{Lk} + I_{pump} + I_{external} + I_{BB})}{C_n + C_{myelin}}$$

$$\frac{dE^*}{dt} = -\frac{I_{Kf^*} + I_{Ks^*} + I_h + I_{pump^*} + I_{Lk^*} - I_{BB} - C_{myelin}\frac{dE}{dt}}{C_{ax}}$$

Capacitance: C_n = 1.4, C_{myelin} = 1.55, C_{ax} = 327 *pF*

Ion concentrations: $[Na]_i$ = 9, $[Na]_o$ = 144.2, $[K]_i$ = 155, $[K]_o$ = 4.5 *mM*

Sodium current:

$$I_{Na} = P_{Na}(m^3h)z(Na)$$

$$I_{NaP} = P_{Na}\left(\frac{P_{Na_P}}{100}m_p^3\right)z(Na)$$

$$z(Na) = \frac{EF^2}{RT}\left(\frac{Sel_{Na}\{[Na]_o - [Na]_i\exp(\frac{EF}{RT})\} + (1 - Sel_{Na})\{[K]_o - [K]_i\exp(\frac{EF}{RT})\}}{1 - \exp(\frac{EF}{RT})}\right)$$

Fast potassium current:
$I_{Kf} = G_{Kf}n^4(E - E_{Kf})$
$I_{Kf^*} = G_{Kf^*}n^{*4}(E^* - E_{Kf})$

Slow potassium current:
$I_{Ks} = G_{Ks}s(E - E_{Ks})$
$I_{Ks^*} = G_{Ks^*}s^*(E^* - E_{Ks})$

Leak current:
$I_{Lk} = G_{Lk}(E - E_r)$
$I_{Lk^*} = G_{Lk^*}(E^* - E_r^*)$

Barrett-Barrett current:
$I_{BB} = G_{BB}(E - E^*)$

Current through HCN channels:
$I_h = G_hq(E^* - E_h)$

Equilibrium potentials: $E_x = \frac{RT}{F}\ln\left(\frac{[K]_o + Sel_x[Na]_o - Sel_x[K]_o}{[K]_i + Sel_x[Na]_i - Sel_x[K]_i}\right)$ *for* $x = K_f, K_s, h$

$$Sel_{Na} = 0.9,\ \ Sel_{Kf}, Sel_{Ks} = 0,\ \ Sel_h = 0.097$$

$$\frac{dm}{dt} = \alpha_m(1 - m) - \beta_m m, \text{ and similarly for } m_p, h, n, s, n^*, s^*, q$$

$$\alpha_m, \alpha_{m_p}, \alpha_n, \alpha_s = \frac{A(E - B)}{1 - \exp((B - E)/C)}$$

$$\alpha_h, \beta_m, \beta_{m_p}, \beta_n, \beta_s = \frac{A(B - E)}{1 - \exp(\frac{E - B}{C})}$$

$$\beta_h = \frac{A}{1 + \exp(\frac{B - E}{C})}$$

$$\alpha_q = A\exp((E - B)/C)$$

$$\beta_q = A/\exp((E - B)/C).$$

	A (ms^{-1}, at 36°C)	Q10	B (mV)	C (mV)
α_m	6.54	2.2	−18.5	10.3
β_m	0.302		−22.8	9.16
α_{m_p}	3.27		−36.5	10.3
β_{m_p}	0.151		−40.8	9.16
α_h	0.126	2.9	−115.1	15.6
β_h	8.60		−32.9	19.0
α_n	0.0221	3.0	−90.8	7.7
β_n	0.0393		−73.6	7.35
α_s	0.00563		−23.5	12.7
β_s	0.00341		−91.1	11.7
α_q, β_q	0.00522		−107.3	−12.2

*Denote internodal properties

Voltage- and time-dependent parameters for the rate constants, α and β for human motor axons.